ADVANCED MATERIALS INTERFACES
www.advmatinterfaces.de

Interaction of Layered Silicates with Biomembranes: Ion Exchangers and Non-Exchangers

Stefania Cananà, Cristina Pavan, Chiara Bellomo, Guillermo Escolano-Casado, Giuseppe Chilla, Dominique Lison, Lorenzo Mino, and Francesco Turci*

Layered silicates (LS, clays) are a composite group of minerals whose industrial interest and technological applications are progressively expanding, spanning from catalysis to biomedicine. However, the compatibility of LS with biological systems is not clear, and mechanistic data about biophysicochemical interactions at the interface of LS and biomembranes are scarce. Here, cell membrane damage, assessed using red blood cells as model membranes, is revealed for kaolin (> 75 wt.% kaolinite, 1:1 layer structure) and bentonite (> 90 wt.% montmorillonite, 1:2 layer structure) particles. The high membranolytic capacity of bentonite (i.e., high ion-exchanger LS) is the result of the combined contribution of both mineral surface features and sample-specific cation exchange capacity (CEC). For kaolin (i.e., non-ion-exchanger LS), the capacity to damage membranes is primarily due to surface hydroxyl species, that is, silanols and aluminols, exposed at the crystal lattice boundaries. When kaolin is thermally disorganized into amorphous metakaolin, membrane damage is driven by a specific sub-population of surface hydroxyl species, namely the "nearly free silanols", previously evidenced on quartz. This study establishes the rationale underlying the interactions between LS particles and membranes and can set the basis for the understanding of interfacial phenomena of LS.

1. Introduction

Layered silicates (LS, clays) are a heterogeneous group of minerals ubiquitous on Earth, which constitute a major mineral resource for the industry worldwide.[1] LS possess unique properties, including high surface area to unit weight ratio, high porosity, adsorption, cation exchange capacity (CEC), and surface chemical functionalities, including charge and hydroxyl groups (–OH), which are essential for many industrial applications. Advances in technology on (nano-)clays improved the many uses of LS-based products from traditional ceramics to innovative functional nanocomposites. In recent years, LS are gathering attention for new potential applications for use in sustainable energy, green environment, and biomedicine. Processing and technological modifications of LS minerals determined their use as adsorbents,[2] catalysts,[3] and biomaterials.[4] They are used as fillers and gellants in paint, plastic,[5] and in food packaging,[1b,4,6] as rheology modifiers in cosmetics and pharmaceutics,[7] and as adsorbents in wastewater treatment.[8] Advanced LS-based nanomaterials are being studied as drug delivery systems,[9] bioimaging probes,[9c,d] bone tissue engineering materials,[10] and antibacterial agents.[11] Considering the growing use and the new applications of LS also in the biomedical field, the understanding of the biophysicochemical interactions at the LS–bio interface is crucial for addressing possible adverse effects on human health and developing safe-by-design nanocomposite materials.

If compared to other largely investigated particles and nanomaterials, such as silica, the mechanisms of interaction of LS particles with biosystems and the LS physicochemical features leading to the crosstalk with biomolecules have been poorly defined.[12] These features may induce detrimental effects on biomolecules or contribute synergically when LS are in association with toxic minerals, such as quartz (QZ) which is often present in clays. Thus, mechanistic knowledge of the biophysicochemical interactions of LS would also be crucial in complementing the eco-exposome to mineral dusts, to determine the primary risk drivers in complex mixtures.[13] LS particles and their derived nanocomposites are generally considered biocompatible, promoting cell adhesion and proliferation.[9c,10a] However, concerns regarding the possible cell damage caused by LS

S. Cananà, C. Pavan, C. Bellomo, F. Turci
Department of Chemistry
"G. Scansetti" Interdepartmental Centre for Studies on Asbestos and Other Toxic Particulates
University of Turin
Via Giuria 9, Turin 10125, Italy
E-mail: cristina.pavan@unito.it
C. Pavan, D. Lison
Louvain Centre for Toxicology and Applied Pharmacology
Université catholique de Louvain
Avenue Hippocrate 57, Brussels 1200, Belgium
G. Escolano-Casado, G. Chilla, L. Mino
Department of Chemistry
Nanostructured Interfaces and Surfaces Interdepartmental Centre
University of Turin
Via Giuria 7, Turin 10125, Italy

The ORCID identification number(s) for the author(s) of this article can be found under https://doi.org/10.1002/admi.202201347.

DOI: 10.1002/admi.202201347

have been raised, especially on kaolin and bentonite aluminosilicates.[12b,c,14] In vitro studies showed that kaolin and bentonite are cytotoxic to a variety of mammalian cells, including macrophages, lung epithelial, and endothelial cells.[12,14a,15] Among primary mechanisms of cellular toxicity, both kaolin and bentonite have been shown to induce cell membrane damage,[16] oxidative stress in acellular,[17] and in vitro tests,[18] metabolism impairment, and DNA damage,[6] with varying intensity of the effects depending on the LS type and the test conditions.

The composition and physicochemical characteristics of the LS were suggested to influence cell toxicity, however, studies available in this direction are scarce. Surface groups, that is, charged sites and hydroxyl groups, including silanols (Si—OH) and aluminols (Al—OH), have been proposed as sites of interaction between LS and biomolecules. By masking these surface groups with dipalmitoyl phosphatidyl choline (DPPC), poly-2-vinyl pyridine-N-oxide (PVPNO), and positively charged molecules (e.g., methylene blue, paraquat), a decreased cell damage was observed for both kaolin and bentonite. These results suggested that LS surface plays a role in the membranolytic effect.[19] The leaching of LS structural metal ions (e.g., Si, Al) in cellular media, also raised concerns because of the possible membranolytic and cytotoxic activity of Al^{3+}.[11,20] In addition, the CEC of some clays may generate local ionic imbalances that can alter cellular homeostasis.[21] Recent in vitro and in vivo studies questioned against a common hazard mechanism of aluminosilicates, as a varying degree of toxic effects have been found with exposure to kaolin and bentonite particles.[14a] Kaolinite and montmorillonite share a similar chemical structure, platelet-like morphology, and size. However, chemical peculiarities related to their crystal structure, including adsorption capacity and CEC, and surface characteristics, may strongly differentiate the two LS sub-groups and promote different molecular interaction mechanisms with membranes and biomolecules.

Among mineral LS, this study is focused on kaolinite and montmorillonite, as the most promising aluminosilicates with potential use in biomedical applications. Kaolinite is a 1:1 phyllosilicate of the chemical formula $Al_2Si_2O_5(OH)_4$, which has a layer structure made up of tetrahedral silica and octahedral alumina (TO) sheets (**Figure 1**d). Montmorillonite is a 2:1 phyllosilicate of silica-alumina-silica (TOT) sheets (Figure 1h), and its chemical formula is $(M^+, 1/2\ M^{2+})_x\ (Al_{4-x}\ Mg_x)Si_8O_{20}(OH)_4$, where $M^+ = Na^+, K^+$, $M^{2+} = Mg^{2+}$, or Ca^{2+}, and ideally the degree of isomorphous substitution is x = 0.33.[22] The exposed planar surfaces of these three-LS consist of siloxanes (Si—O—Si), while for kaolinite, the planar surfaces equally expose siloxanes and hydroxylated alumina. In the case of kaolinite, substitution in the lattice is not frequent, thus the charges within the structural units are balanced and the layers are electronically neutral. In montmorillonite, the isomorphic substitution in the O sheets (e.g., aluminum by magnesium, iron, lithium, zinc, chromium, or nickel) creates an excess of negative structural charge that is delocalized on the oxygens of the basal surface. This charge is compensated by exchangeable hydrated cations in the interlayer space (mainly, Na^+, Ca^{2+}, K^+, and Mg^{2+}), which also contribute to bonding the layers. For montmorillonite, the interlayer space width is ca. 1–2 nm or more, and is filled by water and counterions. This is possible because the layers are bound through weak van der Waal's forces and the net negative charge

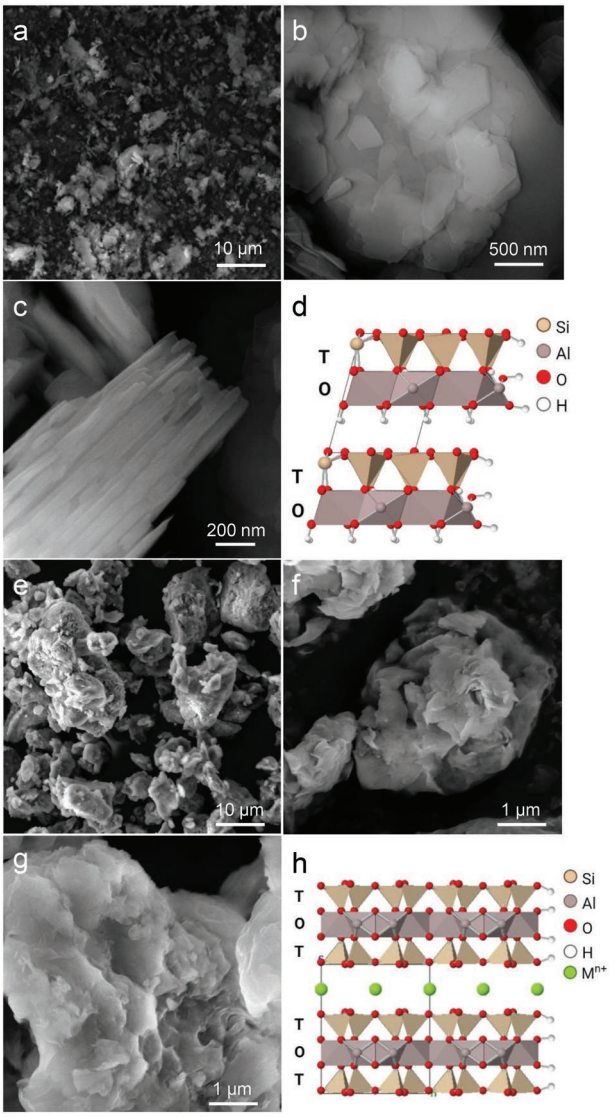

Figure 1. Morphology and crystal structure of kaolin and bentonite particles. Micrographs obtained by FE-SEM imaging of a–c) K3 and e–g) B2. Magnification: (a, e) × 5k, (b, f) 100 and 70k, respectively, and (c) × 200k. Crystal structure of d) kaolinite[26] and h) montmorillonite,[27] where broken edge OH groups (i.e., silanols and aluminols) are evidenced.

deficiency of the basal planes determines strong hydration capability, especially for the so-called Na-bentonite. The structure of kaolinite does not present an interlayer space. The layers are electronically neutral, and the bonding between layers occurs through hydrogen bonds.[23] The interaction among layers is hence stronger than in bentonite, and the occurrence of water molecules or cations in the interlayer space is not necessary to the structural stability of the clay.

Our recent findings indicate that a specific distribution of surface OH located at a well-defined distance (i.e., nearly-free silanols, NFS) is responsible for the membranolytic and inflammatory activity of silica particles.[24] We hypothesized that a mechanism of membrane damage driven by surface OH moieties might also exist for kaolin and/or bentonite particles. Here, the capacity of kaolin and bentonite particles to cause membrane lysis was assessed, and their mechanism of action was

compared. Four kaolin (> 75 wt.% kaolinite) and four bentonite (> 90 wt.% montmorillonite) particles from different extraction sites were included in the study, in order to increase the representativeness of the study. The capacity of these LS particles to interact with membranes was assessed using red blood cells (RBCs) membranolysis assay. RBCs are a simple model of non-internalizing cells that can be conveniently employed in the understanding of the biophysicochemical interactions occurring between biological membranes and mineral surfaces.[25] For membranolysis tests, a micrometric QZ sample and amorphous nanometric silica (AS) were used as reference particles because of their well-documented membranolytic activity that has been related to NFS.[24] Particles were characterized for their bulk physico-chemical properties and IR spectroscopy was carried out to inspect the surface OH groups. To investigate possible structure-activity relationships, the surface OH moieties of one kaolin sample were modulated by thermal treatments, and the membranolytic activity of the surface-modified kaolin was assessed. Moreover, to reveal if ion exchange is involved in the membranolytic mechanism of kaolin and bentonite particles along with surface sites, membranolysis induced by particle leachates was also tested.

2. Results and Discussion

2.1. Physicochemical Characterization of Kaolin and Bentonite Particles

A panel of four kaolin (K1-4) and four bentonite (B1-4) samples were characterized for their mineralogical (**Table 1**) and chemical (Table S1, Supporting Information) composition. Among kaolin samples, two were China clays containing mainly kaolinite (K1 and K3, 92 and 96 wt.%, respectively), with some minor amounts of feldspar, illite, and QZ (ca. 1 wt.%). K2 and K4 contained an average of ca. 75 wt.% of kaolinite, and accessory phases which were mainly illite (about 15 wt.%), QZ (especially K2, 11 wt.%), and feldspar (ca. 3 wt.%). Among bentonite samples, B2 and B3 contained the larger amount of montmorillonite (≥ 95 wt.%), while B1 and B4 contained ca. 86 wt.% and 73 wt.%, respectively. Minor accessory phases consisted in QZ (0.5–3%), illite (especially in B4), feldspar, calcite, dolomite, and opal. B1 is a natural non-activated Ca-bentonite (low content of Na), B2 a natural Ca-bentonite activated with soda ash (high content of Na), B3 a natural Na-bentonite, and B4 a Na-activated Ca-bentonite (both with high content of Na) (Table S1, Supporting Information).

Morphological analysis of LS particles is reported in Figure 1 for kaolin K3 (Figure 1a–c) and bentonite B2 (Figure 1e–g), taken as example of the 1:1 (Figure 1d) and 2:1 phyllosilicate structure (Figure 1h), respectively. These two samples were selected among others because of their highest purity and low QZ content (Table 1). LS in dried powder is assembled into clusters or agglomerates to form secondary particles ranging from some hundred nanometers to a few micrometers (Figure 1a,e). Agglomeration was particularly evident for bentonite particles which formed larger clusters with respect to kaolin and primary particles were less distinguishable. Platelet-like primary nanoparticles were observed on the surface of the agglomerates.

Table 1. Mineralogical composition of kaolin and bentonite particles.[a)]

Phase [wt.%]	K1	K2	K3	K4	B1	B2	B3	B4
Kaolinite	92	73	96	77	–	–	–	–
Montmorillonite	–	–	–	–	86.3	93–95	96	73
Quartz	1	11	1	2.7	< 0.5	0.5–1	2	3
Illite/mica	4	14	–	16	–	–	1	15
Rutile	–	1	–	0.2	–	–	–	–
Anatase	–	1	–	–	–	–	–	–
Feldspar	3	–	3	2.7	Traces	3–4	1	4
Smectite	–	–	–	0.9	13	–	–	–
Calcite	–	–	–	–	0.1	1–2	–	1
Dolomite	–	–	–	–	–	–	–	1
Opal	–	–	–	–	–	–	–	3

[a)]Carried out on the supplied material by XRD analysis.

K3 showed tiny sheets with pseudohexagonal morphology and well-defined edges (Figure 1b,c). The individual sheets were stacked to form aggregates of different sizes that exposed irregular and sharp edges. B2 presented irregular and thin flakes with less defined edges (Figure 1f,g). These flakes realize face-face interactions that led to dense aggregates of varying sizes and pseudo-spherical morphology.

Dry kaolin samples showed a total specific surface area (SSA) lower than bentonite samples (**Table 2**; Brunauer, Emmett, and Teller (BET) method using nitrogen adsorption, N_2-BET). Adsorption-desorption isotherm of kaolin samples did not exhibit hysteresis in the range $0.4 \leq P/P_0 \leq 0.98$ (Figure S1, Supporting Information), indicating the absence of mesopores (2–50 nm). Micropore area was negligible on kaolin samples, and the external specific surface area (SSA_{ext}), which is the outer area available for establishing interactions with cells and biomolecules, could be reasonably approximated to the total SSA_{TOT}. All bentonite samples showed variable micropore area, ranging from negligible to ca. 40% of the total area (B4 and B2, respectively). Taking into account that the N_2-BET method of clay minerals does not measure the interlayer space,[28] the SSA_{ext} of bentonite samples can be derived by subtracting the micropore area from the SSA_{TOT}[29] (Table 2). The SSA of the reference non-porous silica particles QZ and AS was 5 and 50 $m^2\ g^{-1}$, respectively.

The hydrodynamic diameter (Z-average) and ζ potential of kaolin and bentonite particles in ultrapure (MilliQ) water and 0.01 M phosphate buffer solution (PBS) were measured by dynamic and electrophoretic light scattering (DLS/ELS), and are shown in **Figure 2** and Table S2, Supporting Information.

Table 2. SSA and micropore area.

$m^2\ g^{-1}$	K1	K2	K3	K4	B1	B2	B3	B4	QZ	AS
SSA_{TOT}[a)]	15	22	13	12	65	91	46	21	5	50
Micropore Area[b)]	2	–	–	–	19	35	15	1	–	–
SSA_{ext}[c)]	13	22	13	12	47	56	31	20	5	50

[a)]Measured by BET method using N_2 adsorption; [b)]from *t*-plot method; [c)]obtained by subtracting the micropore area from the total SSA.

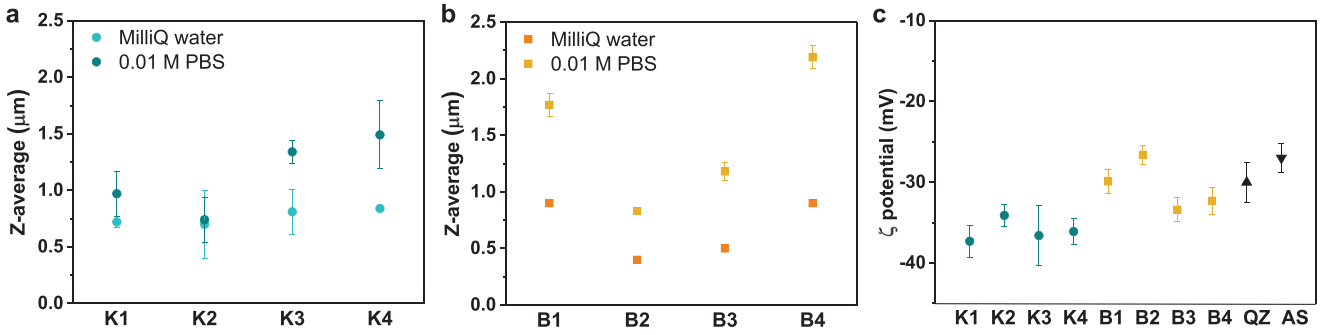

Figure 2. Hydrodynamic diameter (Z-average) and ζ potential of kaolin and bentonite dispersions. a) Kaolin and b) bentonite particles were dispersed in ultrapure water or 0.01 M PBS milieu (2 mg mL^{-1}), sonicated for 1 min with an ultrasonic probe, and Z-average was assessed by DLS on diluted dispersions (0.2 mg mL^{-1}). c) ζ potential of kaolin (circle) and bentonite (square) particles sonicated, dispersed (0.1 mg mL^{-1}) in 0.01 M PBS (pH 7.4), and assessed by ELS. Values are means ± standard deviation (SD). The data of QZ and AS are reported as reference (triangle).

DLS analysis of kaolin and bentonite particles (Figure 2a,b) dispersed in ultrapure water indicated that samples formed highly heterogeneous suspensions (polydispersity index ranging from 0.4 to 0.9), with average size of about 0.7–0.8 µm for kaolin particles, and variable values for bentonites. Among bentonites, B2 showed the lowest average hydrodynamic diameter (ca. 0.36 µm), and B1 and B4 the highest (ca. 0.90 µm). Dispersion of LS particles in 0.01 M PBS generated suspensions containing larger agglomerates compared to ultrapure water dispersions, which often attained average hydrodynamic size above 1 µm. This may indicate that these particles tend to agglomerate as a possible result of ionic strength variation.

The ζ potential measurements (Figure 2c), showed that all samples were negatively charged at physiological pH (7.4), in the same milieu used for membranolysis assessment (0.01 M PBS). Kaolin particles showed ζ potential values (ranging from ca. −34 to −37 mV) slightly lower than bentonite particles (from ca. −33 to −27 mV). These values are in line with previous studies,[14a] which reported a net negative charge for both bentonite and kaolin samples, with variable values depending on the milieu in which the particles are suspended. The net negative surface charge at pH 7.4 may be due to the presence of ionizable surface hydroxyls at edges, that is, Si—OH and Al—OH, and Al—OH of the octahedral basal plane in kaolin. These moieties are pH-dependent, non-permanent charges. The silanol groups contribute only to the negative charge, through the formation of $Si—O^-$ surface complexes by deprotonation. The aluminol groups are amphoteric in nature and can be protonated ($Al—OH^{2+}$) and deprotonated ($Al—O^-$) at low and high pH, respectively. At pH 7.4, aluminol sites on edges and octahedral basal faces are expected to be largely deprotonated as the pH is higher than their point of zero charge.[30] In addition, permanent negative charges on silica basal plane, due to isomorphic substitution and charge deficiency, may contribute to the net negative charge of both kaolin and bentonite.

2.2. Kaolin and Bentonite Particles Show High Membranolytic Activity

The membranolytic activity (% hemolysis) of the kaolin and bentonite samples as a function of increasing particle concentration is reported in **Figure 3**a,b, respectively.

All four kaolin samples showed a marked membranolytic activity (Figure 3a), which was comparable to that of the reference QZ, both in terms of intensity and dose-response trend. In our samples, the occurrence of QZ is very low (< 3 wt.%, Table 1) and a significant contribution to the membranolytic activity from this mineral should be ruled out, except for K2 (11 wt.%). Since early studies,[16a] aluminosilicates were claimed responsible for the membranolytic caused by several clays, and this phenomenon was not related to the occasional presence of QZ. Similarly, we did not observe a correlation between LS membranolytic activity and the content of accessory mineral phases, including QZ and illite. A clear dose-effect membranolytic activity was evident for all the kaolin samples. K1 and K2 samples appeared slightly more membranolytic than K3 and K4, as they induced significant hemolysis at a lower dose (0.16 mg mL^{-1}, Figure 3a'), and were more hemolytic at the highest concentration (15 mg mL^{-1}) compared to the other two samples. A strong membranolytic activity was also observed for all the four bentonite samples (Figure 3b) already at a very low concentration (i.e., 0.05 mg mL^{-1}, Figure 3b'), which is non-hemolytic for kaolin and QZ, but strongly hemolytic for the nanosilica (AS).[24] This suggests that the nanostructured surface and higher SSA of bentonites may increase the interaction with RBCs, as it is reported for AS. All the bentonite samples reached a maximal (100%) hemolytic activity at the concentration as low as 10 mg mL^{-1}, B3 showing the most rapid increase at low concentrations (Figure 3b'). While AS showed a regular concentration-dependent increase up to 1.2 mg mL^{-1}, this trend was less evident for bentonites, which showed plateau effects, particularly evident for B3. B3 reached a plateau already at 0.078 mg mL^{-1} and then increased and reached 100% hemolytic activity at 10 mg mL^{-1}. These results suggest that the membranolytic effect of bentonites on RBCs may not be exclusively dependent on a particle surface interaction phenomenon, which would be concentration dependent as observed for AS, but that other bentonite-specific factors may contribute.

The stronger membranolytic activity of bentonite compared to kaolin was highlighted by extrapolating the EC50, that is, the concentration of particles inducing 50% of the hemolytic activity, from the non-linear dose-response curve fitting of the hemolysis data reported as logarithmic concentrations (Figure S2, Supporting Information). Bentonite samples were about ten

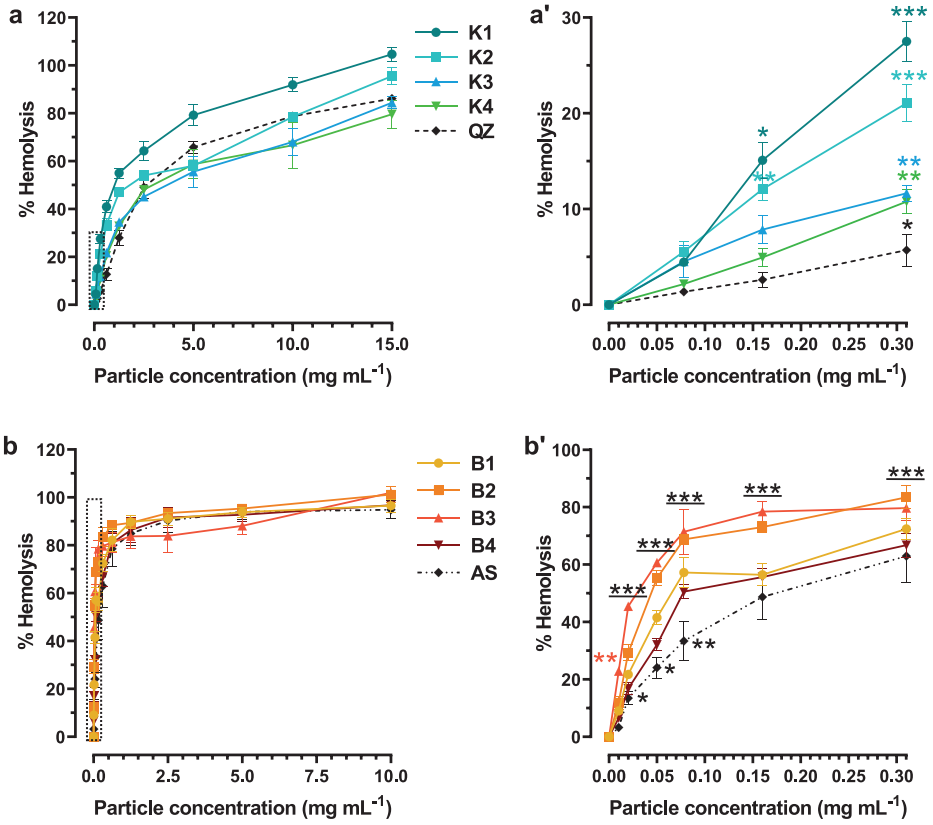

Figure 3. Membranolytic activity of kaolin and bentonite particles. Increasing concentrations of a) kaolin and b) bentonite particles were incubated for 30 min with purified sheep RBCs. QZ and AS were used as positive reference particles in each set of data, respectively. The insets (a' and b') show hemolysis of low concentrations (≤ 0.3 mg mL^{-1}) of particles. Values reflect the fraction of the total hemoglobin content released and are reported as mean ± SEM of three independent experiments. Data were analyzed with one-way ANOVA, followed by Dunnett's post-hoc test. *$p < 0.05$, **$p < 0.01$, and ***$p < 0.001$ versus control not exposed to particles.

to one hundred times more active than kaolin. The higher membranolytic activity of bentonite samples could be only partially attributed to their higher SSA_{ext}. In fact, no linearity between EC50 and SSA_{ext} was observed (Figure S2c, Supporting Information). It should be remarked on the limitations of the gas adsorption BET method to measure the SSA_{ext} of these materials. While the SSA_{ext} of non-swelling kaolin remains generally valid when the material is dispersed in water and may be used to discuss adsorption phenomena at the solid-liquid interface, the SSA_{ext} of bentonite may vary in suspension, due to swelling and agglomeration or flocculation.[28] DLS analysis of bentonite samples dispersed in PBS (Figure 2b and Table S2, Supporting Information) showed the formation of large agglomerates, thus the available surface area for interaction with RBC could be much lower than the measured SSA_{ext}.

2.3. The Membranolytic Activity of Bentonite is Due to Cation Exchange Capacity

We considered that the CEC of LS particles may influence the ionic strength of the milieu, and possibly indirectly damage the RBC membrane. To test this hypothesis, we assessed the membranolytic activity of the particle leachates. Particles were pre-incubated for 30 min in the same conditions used for hemolysis test, but without RBCs. Leachates were cleared by centrifugation, and filtrated. Particle-free leachates were contacted with RBCs. **Figure 4**a shows the membranolytic activity of the kaolin and bentonite leachates superimposed on the membranolytic activity induced when the same concentration of particles is directly put in contact with RBCs. The supernatants of QZ and AS were comparatively assessed, assuming that these two silica samples are not able for cation exchange or significant ion release in the experiment timespan. For the kaolin leachates, no hemolysis was observed, except for K1, whose leachate showed a membranolytic activity of ca. 30%. We concluded that membranolytic activities of kaolin samples, but K1, are mediated by a direct interaction between RBC and clay surface. In fact, as the particle concentration (15 mg mL^{-1}) used to test K1 leachate induced 100% of hemolysis (Figure 3a), it might be inferred that approximately 70% of the lytic interaction of K1 is particle-mediated, while the remaining 30% is attributable to indirect damage due to ionic strength alteration of the milieu. Contrary to kaolin, all bentonite leachates showed a strong hemolytic activity (Figure 4a), with respective activities in the following order: B2 (82%) > B3 (71%) > B1 (50%) > B4 (35%). These results suggest that a significant fraction of the membranolytic outcome of bentonite may be due to the indirect effect of the

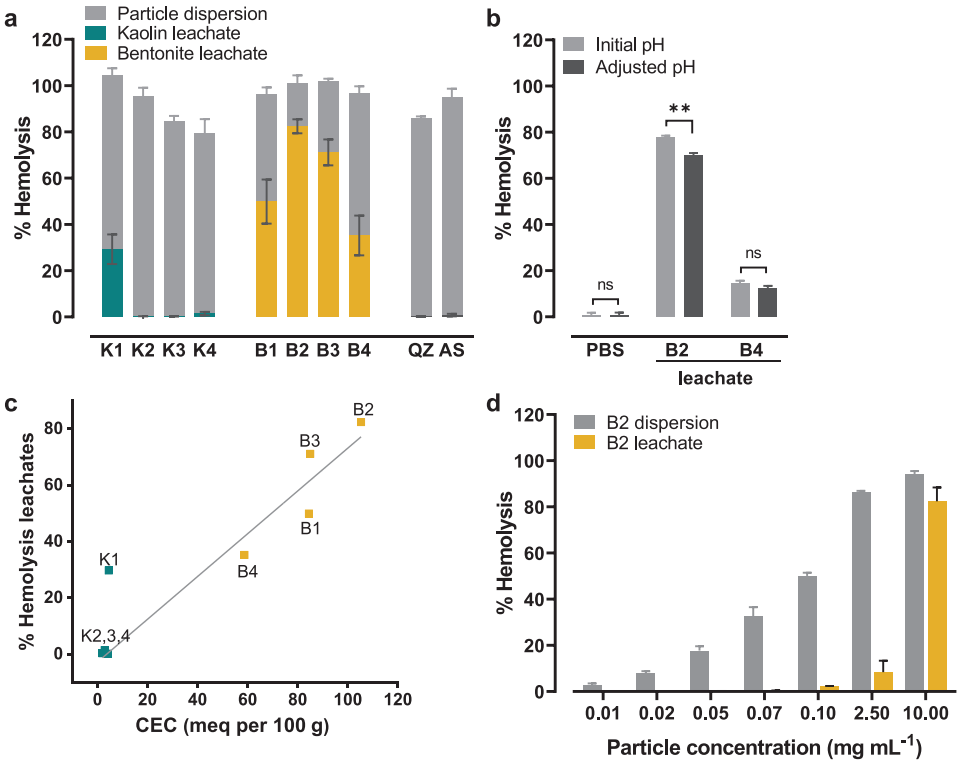

Figure 4. Membranolytic activity of kaolin and bentonite leachates in relation to particle CEC. Filtrated supernatants were collected after incubation of the particles (15 mg mL^{-1} for kaolin and QZ, and 10 mg mL^{-1} for bentonite and AS) in 0.01 M PBS for 30 min and contacted with RBCs. a) Hemolytic activity of the kaolin and bentonite leachates compared with the hemolytic activity induced by direct contact of the particles at the same concentration. QZ and AS were used as references. Values are means ± SEM of four independent experiments. b) Hemolytic activity of PBS (negative control), B2 leachate, and B4 leachate adjusted with NaOH or HCl to verify possible hemolysis induced by pH variations. PBS: init. pH, 7.4; adj. pH, 9; B2 leachate: init. pH, 8.9; adj. pH, 7.4; B4 leachate: init. pH, 8.2; adj. pH, 7.4. Values are means ± SEM of three independent experiments. Data were analyzed with two-tailed Student's t-test. $^{**}p < 0.01$ initial versus adjusted pH. c) Correlation between CEC (meq per 100 g) and % hemolysis of kaolin and bentonite leachates. Data were compared by linear regression analysis (Pearson's coefficient = 0.98; $R^2 = 0.95$). K1 has been excluded from analysis because considered an outlier. d) Hemolytic activity of bentonite B2 dispersion or leachate at increasing doses.

cations exchanged by the clay with the milieu. While for B1 and B4 particles the hemolytic activity appeared partially affected by their capacity to induce alterations in the culture milieu, for B2 and B3 the alterations in the milieu played the predominant role in the hemolytic activity of the particles, which may also explain the poor dose-response relationship exhibited by B3 (Figure S2a,b, Supporting Information).

To better define the causal effect of cation exchange promoted by bentonite samples, we verified possible variation of the pH of the milieu (Table S3, Supporting Information), which could be an index of ionic imbalances. For kaolin, no variations with respect to the physiological pH of the milieu (0.01 M PBS, pH 7.4) were observed, while for B2, B3, and B4 pH increased up to 8–9, which overcame the buffering capacity of PBS. Basification was particularly significant for B2 and B4, the two bentonites which were activated with soda ash (Na_2CO_3). These results were congruent with the high basification effect of bentonites in water, especially for B2 and B4 (Table S3, Supporting Information). However, the observed pH variations did not explain the RBC lysis elicited by bentonite (Figure 4b). Indeed, when PBS pH was adjusted to pH = ca. 9, the hemolytic activity of the alkaline milieu was negligible, as recorded for PBS at physiological pH. Further proof of the lack of pH-dependent hemolytic effect was obtained by adjusting the basic leachates of B2 and B4 to 7.4. The hemolytic activity of acidified B4 leachate was identical to the basic leachate, and only a slight, even if significant, reduction for B2 leachate was observed. The membranolytic effect should hence be due to the unbalance of cations other than H^+.

We assessed the CEC of the samples (Table S3, Supporting Information). Both kaolin and bentonite can exchange cations adsorbed on their surface with the surrounding milieu, albeit bentonite CEC is usually higher than kaolin.[22a] As expected, the CEC of all kaolin samples (2–4.5 meq per 100 g of clay) was considerably lower than that of bentonite (60–100 meq per 100 g of clay). CEC values well-correlated with the membranolytic activity of the particle leachates (Figure 4c). K1 leachate high hemolytic activity was accompanied by a low CEC, positioning the kaolin as an outlier from the correlation between hemolysis and CEC. This may be due to other features not strictly related to CEC, possibly to the dissolution of accessory mineral phases. To gain evidence on the cations dissolved/exchanged, we also assessed the concentration of some cations (i.e., Mg, Ca, Si, Al) in the cellular milieu by inductively coupled plasma

optical emission spectroscopy (ICP-OES) (Table S4, Supporting Information). Due to the high concentration of Na^+ and K^+ in the pristine milieu, it was not possible to directly measure these two ions. The low level of structural Σ(Al+Si) cations in solution, which ranged from 2 to 17 ppm, indicated a negligible particle dissolution, which is consistent with the short incubation time (30 min). However, a higher amount of Σ(Al+Si) = 46 ppm was recorded for K1 and might explain the membranolytic effect shown by the leachate of this sample. Aluminum ions may indeed promote RBC membrane disruption by binding to phosphate groups in phospholipids (PL) as already reported in the literature.[11,20] Bentonite, in general, showed a much higher Mg and Ca efflux in solution, which is compatible with the high CEC of this mineral. In particular, B1 registered a Σ(Mg+Ca) > 200 ppm, likely counterbalanced by the influx of monovalent cations from the buffer (Na^+, K^+, H^+). The alteration of the ionic strength of the milieu induced by the cation exchange of bentonite but not kaolin is likely at the base of the observed membranolytic activity of the bentonite leachates. The high Mg and Ca efflux of bentonites may induce a large decrease of K^+ and Na^+ concentration in the milieu that in turn could affect RBC tonicity. In in vitro studies, the capacity of bentonites to exchange cations, which depends on the specific CEC of each bentonite sample, may be decisive in influencing the ionic strength of the cellular milieu. A similar CEC-mediated effect has been described for erionite fibers in inducing necrosis of macrophages.[32] In the specific case of the hemolysis test, structural integrity of the RBC membrane is very sensitive to variations of osmolarity and extracellular sodium concentrations, which may induce modifications in RBC ion transport, volume, and cell shape, possibly resulting in cell lysis.[33]

Besides CEC-mediated effect, the role of the surface species of bentonite particles in RBC lysis could not be completely ruled out. Indeed, the contribution of the particle surface became predominant at low doses of bentonite, and the leachate contribution was negligible at doses < 2.5 mg mL^{-1} (Figure 4d). For kaolin, only a particle-driven mechanism should be invoked to explain its membranolytic activity.

2.4. Masking Surface Hydroxyl Species Inhibits the LS Membranolytic Activity

The involvement of the particle surface in the interaction with RBCs was then explored with self-assembled 1,2-dioleyl-sn-glycero-3-phosphocholyne (DOPC) and 1,2-dioleoyl-sn-glycero-3-phospho-L-serine (DOPS) PL. DOPC can prevent membranolysis by masking the surface OH species, as it has been shown for silica particles.[16c,31] The hemolytic activity of K3 and B2, in presence of self-assembled DOPC and DOPS structures is reported in **Figure 5**. DOPC and DOPS were used because they share the same apolar tail (i.e., octadecenoyl) and differentiate for the polar head. The polar head of DOPC is a phosphocholine, which is zwitterionic at a physiological pH, while the polar head of DOPS is a phosphoserine, which is negatively charged at pH 7.4 due to an additional carboxyl residue.

DOPC self-assembled structures induced a dose-dependent reduction of the membranolytic activity of both K3 and B2 (Figure 5a). This effect suggests the involvement of the kaolin and bentonite outer OH moieties in membrane damage. The strong affinity of DOPC for the kaolin surface was confirmed by testing the membranolytic activity of DOPC-coated K3 that was washed three times with the milieu prior to incubation with RBCs. Even after washing, the hemolytic activity of DOPC-coated kaolin was quenched (Figure S3, Supporting Information). This finding confirms that DOPC is irreversibly adsorbed on kaolin surface, because of the establishment of a strong chemical interaction between kaolin and DOPC. A similar reduction of the membranolytic activity when the surface of kaolin and bentonite was coated with aluminum-hydroxy and polyvinylpyrrolidone (PVPNO) polymers was

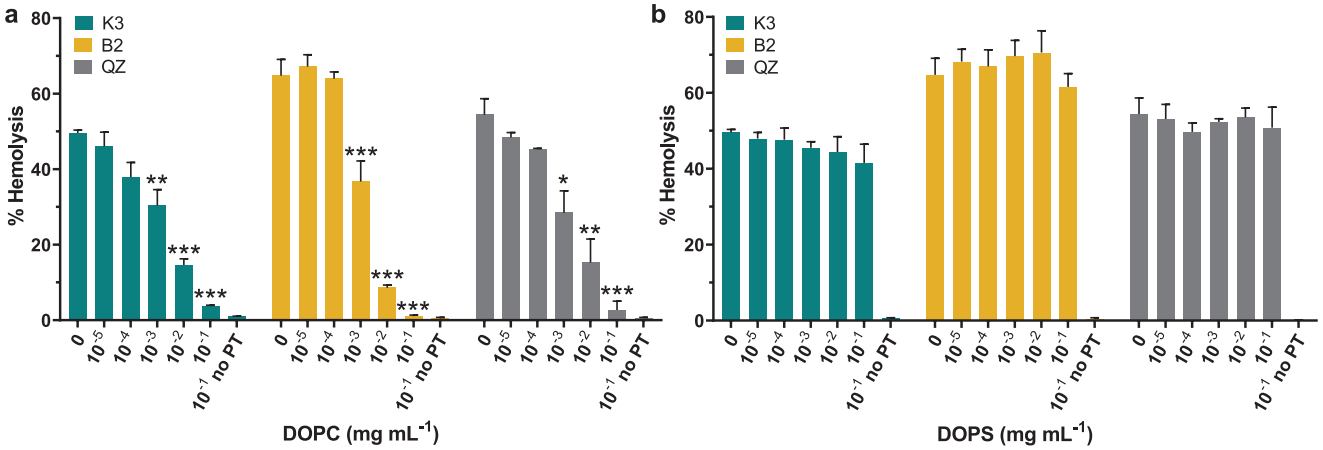

Figure 5. Membranolytic activity of kaolin and bentonite particles in presence of self-assembled PL. K3, B2, and QZ (positive reference QZ) at their respective EC50 (3.0, 0.043, and 2.8 mg mL^{-1}, respectively) were pre-incubated with just the vehicle (0 mg mL^{-1}) or increasing concentrations (from 10^{-5} to 10^{-1} mg mL^{-1}) of self-assembled a) DOPC or b) DOPS for 30 min. A suspension of 5% RBC was added and the hemolytic activity was assessed after a further incubation of 30 min. "No PT" corresponds to groups without particles, containing only 10^{-1} mg mL^{-1} self-assembled phospholipid structures. Values are means ± SEM of three independent experiments and were analyzed with one-way ANOVA, followed by Dunnett's post-hoc test. *$p < 0.05$. **$p < 0.01$. ***$p < 0.001$ versus group containing only silica.

reported in previous studies.[34] The authors suggested that the coating may prevent the silanol groups on particle edges from contacting the erythrocyte membrane. Moreover, markers of acute lung inflammation were reduced for LS modified with organic compounds.[15b,35] We recently demonstrated on silica that DOPC, but not DOPS, is irreversibly adsorbed, and this interaction specifically masks NFS, which are held responsible for silica membranolytic effect.[31] For kaolin, the involvement of the exposed outer OH in the interaction with DOPC was further confirmed by FT-IR spectroscopy (Figure S4, Supporting Information).

Conversely, negatively-charged DOPS structures of the same size as DOPC[31] did not alter the hemolytic activity of K3 and B2, revealing that DOPS likely does not interact with the surface of these two LS. Both K3 and B2 are negatively charged in the physiological milieu used for experiments (Figure 2c), due to deprotonated silanols and aluminols. Thus, DOPS, which display a net negative charge, may not interact with kaolin and bentonite surfaces due to electrostatic repulsion. However, also RBCs show a negative ζ potential of ca. −31.8 mV at pH 7.4[36] because of deprotonation of sialic acid residues. This implies that the interaction between kaolin and bentonite particles with RBCs must overcome the electrostatic repulsion, as it occurs for silica.[31] The lack of interaction between LS particles and DOPS may indicate that the role of the $-AlOH_2^+$ proton transfer is not relevant in our studied system, although it might play a role at a more acidic pH.[37]

2.5. Thermal Treatments Modulate Crystal Structure, Surface Hydroxyl Species, and Membranolytic Activity of Kaolin

To gain a detailed view of the origin of kaolin membranolytic effect, a set of thermally treated kaolin was created by heating pristine K3 sample at temperature (T) ranging from 200 to 1000 °C for 2 h in an isotherm oven that was heated with a T ramp of 10 °C min^{-1}. An explorative thermogravimetric analysis (TGA) under a constant heating rate (10 °C min^{-1}) was conducted on pristine kaolin and the expected dehydroxylation path of the clay was observed (**Figure 6**a). At T > 400 °C inner and outer hydroxyl moieties condensed and water was eliminated from the crystal structure. A total weight loss of ca. 12 wt.% was recorded. These findings were corroborated by TGA analysis performed in isothermal conditions for 2h (Figure S5, Supporting Information) at 300, 400, 450, 500, and 600 °C. By heating at $T \leq 400$ °C, the weight loss was almost negligible (0.1–0.2 wt.%). Heating at 450 or 500 °C determined almost half (7 wt.%) of the total weight loss, while at 600 °C the dehydroxylation was complete, with a weight loss comparable to that observed under isothermal conditions (12 wt.%). This

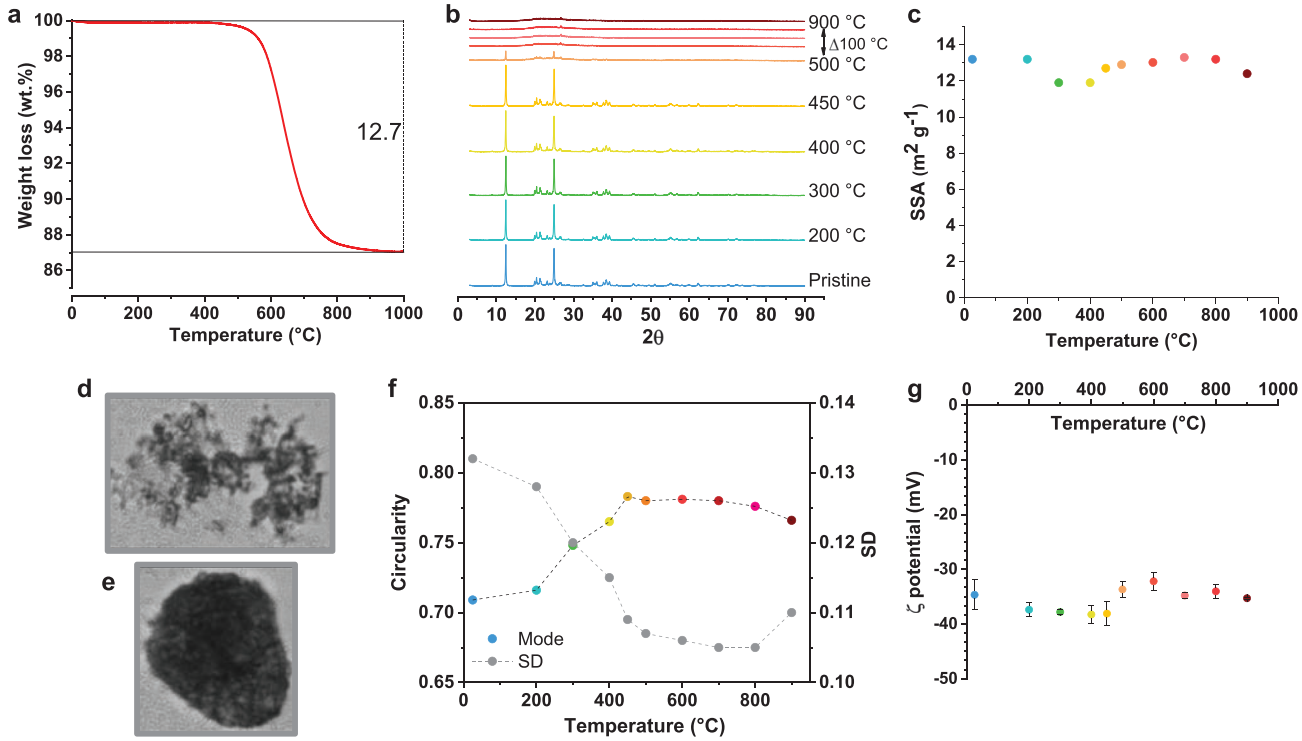

Figure 6. Physico-chemical features of kaolin (K3) calcined at different temperatures. a) TGA of K3 heated up to 1000 °C under nitrogen atmosphere (heating rate 10 °C min^{-1}). An overall weight loss of about 12.7 wt.% was measured. b) X-ray powder diffraction pattern of K3 calcined in a muffle furnace in the T range 200–900 °C in isothermal conditions for 2h (heating rate 10 °C min^{-1}). c) SSA measured by N_2 adsorption. d,e) Morphology of the particle agglomerates of (d) pristine and (e) K3 heated at 500 °C and dispersed in 0.01 M PBS as imaged by FPIA. f) Trend of the mode and standard deviation (SD) of the agglomerate circularity of kaolin heated at different T and dispersed in 0.01 M PBS. g) Z potential of particles dispersed (0.1 mg mL^{-1}) in 0.01 M PBS (pH 7.4).

finding is consistent with the stoichiometry of this hydrated LS. At $T > 800$ °C, the mineral stabilized, and a negligible weight loss was observed up to $T = 1000$ °C, signaling the complete dehydration of the mineral. A change in the crystalline phase accompanied the dehydration process and is commonly described to occur in the 400–650 °C range.[38] Figure 6b reports the X-ray powder diffractograms of the heated kaolin. For treatments at $T \leq 450$ °C the positions and the relative intensities of the diffraction peaks of kaolin were unaltered. This signals that the crystal structure of kaolin was largely preserved below 450 °C. For thermal treatments at $T > 500$ °C a dramatic loss of peak intensity was observed and the formation of metakaolin ($Al_2Si_2O_7$), which has lost the long-range crystal order, characterize the diffractograms collected, as evidenced by the absence of Bragg reflections.[38] This metastable structure still retains the 1:1 layering of the parent kaolinite, although the layers are buckled locally.[39]

Thermal processes, at any tested *T*, slightly affected the SSA (Figure 6c) and the size of particle agglomerates in PBS (Figure S6, Supporting Information). The FE-SEM micrographs of the pristine kaolin and the kaolin heated at 500 and 900 °C (Figure S7, Supporting Information) show sharp and irregular edges made up of tiny sheets. Therefore, thermal treatments do not modify drastically the morphology of the primary particles. However, thermal treatments affected the morphology of the agglomerates that changed from fractal to more densely packed particles (Figure 6d,e, and Figure S8, Supporting Information). By using automated image analysis, the circularity parameter (CP) of particles that were heated at different *T* was obtained (Figure 6f and Figure S9, Supporting Information). The calculation of CP allowed us to quantify the shift from dispersed to close-packed agglomerates of particles. CP is the ratio between the perimeter of the circle having the same area of the particle and the perimeter of the particle. CP value is 1 for a circular particle and decreases as the fractal structure increases. A progressive increase in agglomerate circularity (i.e., more roundish structures) was clearly observed for kaolin heated between room temperature (RT) and 500 °C. Interestingly, treatments at $T \geq 500$ °C were not able to further alter the agglomerate shape.

Despite the surface chemistry of the set of treated kaolin is expected to be largely affected by heating, the overall net charge of the mineral surfaces, described by the ζ potential, was not significantly modified by heating, with values that ranged between −32 and −38 mV (Figure 6g). Thus, despite the reduction of the total amount of OH caused by the thermal dehydroxylation processes, the remaining species exhibited a similar average acidity that confers a similar net charge to the surface.

To further inspect the hydroxyl groups on kaolin, the surface of the K3 sample heated at different *T* was investigated by FT-IR spectroscopy, before and after hydrogen-deuterium (H/D) exchange (**Figure 7**a,b, respectively). Figure 7a reports the FT-IR spectra collected after outgassing the self-supporting pellets of K3 (RT for 120 min). Focusing on the 3800–3400 cm^{-1} spectral region, the OH stretching signal was out of scale for all thermally treated samples between RT and 450 °C. Following heating at $T \geq 500$ °C, the OH pattern was broadened, and its overall intensity was progressively reduced, indicating that the total amount of hydroxyl species was significantly reduced by increasing the *T* of the treatment. In parallel, the triplet of bands at 1930, 1820, and 1730 cm^{-1}, due to the combination of kaolin bulk modes, progressively disappeared. This evidence is in agreement with the expected dehydroxylation process occurring in kaolinite at *T* above 400 °C, which leads to its transformation into disordered metakaolin. Attenuated total reflectance (ATR) infrared spectra (Figure S10, Supporting Information) confirmed the dramatic variation in the bulk and surface properties of the low versus high thermally treated kaolin (for $T > 500$ °C). At low *T*, the bands associated with the OH stretching modes of the inner surface hydroxyls (3684, 3669, and 3651 cm^{-1}) and the inner hydroxyls (3620 cm^{-1})[40] were clearly defined, while at $T > 500$ °C the intensity of the OH signals was drastically reduced and appreciated only in transmission spectra (Figure 7a). Moreover, the well-defined bands attributed to the bulk modes of kaolinite (1150–500 cm^{-1} range) turned into a broad and weaker band centered at ca. 1055 cm^{-1}. These results further confirm the phase transition from kaolin to metakaolin.

Figure 7b reports the OD stretching region (ν_{OD}) of the heated K3 samples after the H/D exchange. The more easily accessible OH groups readily exchange with deuterium forming deuteroxyls (OD), allowing to distinguish the surface from lattice OH groups of kaolinite.[40] Thus, the OD signal was mainly the result of the H/D exchange of outer OH from Al in octahedral sites and silanols and aluminols exposed at the crystal edges, with some minor contribution of inner OH groups during D_2O diffusion inside the lattice. At *T* below the threshold of kaolinite dehydroxylation process (< 400 °C), a complex OD pattern was recorded, in which vibrations typical of structural OH groups of kaolin were assigned at 2706 (outer surface OD) and 2675 cm^{-1} (inner OD).[40] A band at 2758 cm^{-1}, which has been assigned to nearly free silanols (NFS) on silica,[24] was revealed on some heated kaolin samples. At low *T*, when the kaolinite structure prevailed, the band corresponding to the NFS was not well defined, albeit a shoulder was detected between RT and 450 °C (Figure S11a, Supporting Information). At $T \geq 500$ °C, when the metakaolin structure prevailed, the band due to the NFS was clearly appreciated, especially for samples heated at $600\ °C < T < 800$ °C, and then decreased at 900 °C (Figure S11b, Supporting Information). On the 900 °C-treated sample an increase in the broad band (2720–2400 cm^{-1} range) assigned to OH groups engaged in strong mutual inter-silanol interactions was also observed after H/D exchange. This might be assigned to the large phase rearrangement which leads to the formation of Al-Si spinel and segregation of SiO_2 close to this *T*.[39b]

The membranolytic activity of the set of heated kaolin (Figure 7c and Figure S12, Supporting Information) showed almost no significant variation from the pristine sample up to 400 °C. A significant reduction of the membranolytic activity of kaolin was induced by heating at 450 °C, and the lowest activity was attained at 500 °C. By heating at higher *T*, the membranolytic activity progressively increased up to 800 °C, and then rapidly decreased at 900 °C. Mányai and colleagues[41] previously observed a similar trend, and suggested that the degree of hydration of the structure ruled the interaction of the kaolinite particles with erythrocyte membranes. They explained the restoration of membranolytic activity of kaolinite heated at 800 °C with the formation of β-quartz and small amounts of mullite and cristobalite. In our experiments, however, the kaolin sample did not transform in new crystalline phases, as

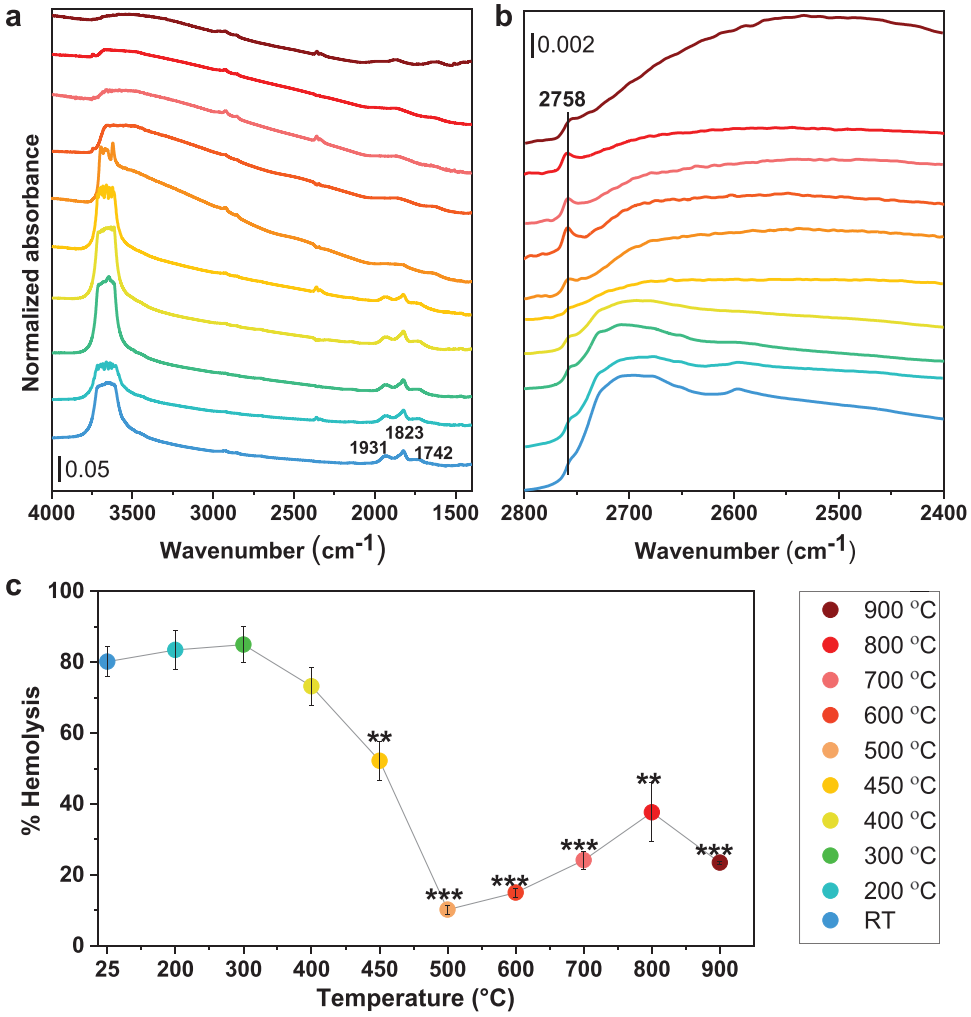

Figure 7. The membranolytic activity of heated kaolin is related to the variation of hydroxyl species. K3 was calcined in a muffle furnace in the *T* range 200–900 °C in isothermal conditions for 2 h (heating rate 10 °C min^{-1}). a) FT-IR spectra of the K3 samples heated at different *T* after outgassing for 120 min at RT. b) FT-IR spectra of the OD stretching region (after H/D exchange) of the K3 samples heated at different *T*. The "OH outgassed spectrum" has been subtracted from all spectra. The peak at 2758 cm^{-1} has been assigned to NFS.[24] c) Hemolytic activity of calcined kaolin at the concentration of 10 mg mL^{-1}. Values are the means ± SEM of three independent experiments and were analyzed with two-tailed Student's *t*-test. $^{**}p < 0.01$. $^{***}p < 0.001$ heated versus pristine sample.

evidenced by XRD analysis, probably because the sample is very pure. This implies that the observed membrane damage can be entirely ascribed to the surface properties of metakaolin. Moreover, membranolysis of the leachates obtained from the series of heated kaolin was completely negligible (Figure S13, Supporting Information), indicating that the mechanism of membrane interaction is surface-mediated, even after transition to metakaolin.

According to the present results, the dramatic variation in membrane damage (Figure 7c) was independent of the slight changes observed for SSA (Figure 6c) and particle size distribution of heated kaolin agglomerates (Figure S6, Supporting Information). However, in the kaolin-metakaolin transition region (RT-500 °C), the decrease in membrane damage might be partially explained by a diminished availability of interaction sites due to the formation of particle agglomerates that exhibited a more circular morphology (Figure 6f). Nonetheless, the increase in circularity can hardly be the main mechanism of action that drives kaolin membranolytic effect. Indeed, when kaolin was heated at $T > 500$ °C the membranolytic activity, but not particle circularity, further varied, indicating that surface species are likely the main molecular drivers of the observed effects.

At pre-transition *T* (< 450 °C) the reduction of the total amount of OH species, which is consistent with thermal condensation and is evidenced by the dramatic decrease of the intensity of the OH stretching band, was not paralleled by any relevant change in membranolytic activity of the differently heated kaolin. This may indicate that membranolysis induced by kaolin particles is not a function of the total amount of surface OH species per se and that some specific exposed OH families may lead to the molecular interaction with membranes. The dramatic decrease in membranolytic activity of the kaolin heated at 450 and 500 °C was accompanied by a reduction in the amount of some outer

OH groups in weak mutual interaction (Figure S11a, Supporting Information, 2750–2660 cm^{-1} spectral range). Together with the variation in particle aggregation/morphology, the loss of weakly interacting OH may account for the observed reduction in membranolytic activity. A similar reduction of the weakly interacting OH groups, which are engaged in the interaction with DOPC, may underlay the reduction in membranolytic activity observed for DOPC-coated kaolin (Figure S4, Supporting Information). From 500 to 800 °C, the increased membranolytic activity of the disordered surface of metakaolin was accompanied by an increase of the signal due to NFS that was described for silica. Finally, at 900 °C NFS reduced, and a reduction of the kaolin membranolytic activity was observed.

It has been described that during the heating of kaolin, the Si-tetrahedral sheets persist in a distorted form, while the Al-octahedral sheets are greatly altered and Al coordination changes.[39b] Up to 400 °C, below OH condensation temperature, only octahedral Al(VI) has been identified by NMR spectroscopy.[39b,42] We may hypothesize that in this state, the outer OH groups of basal and edge surfaces are able to strongly interact with membranes. At *T* causing dehydroxylation of kaolinite, that is, 450–500 °C, pentahedral Al(V) appears with the formation of alumoxyl (−Al=O) groups. This may lead to a reduction of the aluminols on the basal face, which may correlate with the shift of the 2750–2660 cm^{-1} band towards lower ν_{OD}, and is possibly the cause of the reduced affinity for membranes. Above $T > 600$ °C, also tetrahedral Al(IV) occurs, originating covalent sequences Al-O-Al-O. While this species shows the same intensity by rising the *T*, the intensity of the Al(V) increases from 450 to 850 °C, then it decreases and disappears at 980 °C.[42] This trend parallels the intensity of the membranolytic activity of kaolin. Thus, further development of this research might target how the structural rearrangements due to alteration of the coordination state of Al may induce reconstruction of surface species, which are responsible for membranolysis and interfacial phenomena.

In this work, we limited our investigation to the phenomenological interaction of LS with membranes and we defined the molecular nature of this interaction for the OH-specific populations of kaolin. For bentonite, a complex signal from surface hydroxyl species was revealed by FT-IR spectroscopy (Figure S14, Supporting Information). However, the presence of weakly interacting hydroxyl groups including NFS, could not be revealed due to an overlap of many superimposed vibrational features, even after H/D exchange. An ad hoc experimental setup (for instance, the use of molecular probes) should be aimed at discriminating the different components of surface OH groups of bentonites that might interact with PL and cell membrane.

3. Conclusion

Biochemical information on possible mechanisms of interaction between LS particles and cellular membranes is generally scarce. Overall, the physicochemical features that lead the crosstalk of LS with the biological environment are poorly understood. Here, we evaluated the capacity of a set of kaolin (1:1 layer structure, non-ion-exchangers) and bentonite (1:2 layer structure, ion exchangers) particles to damage RBCs, used as model membrane systems. Both kaolin and bentonite samples were highly membranolytic. The membranolytic activity of kaolin samples, except for K1 in which high dissolution of Al^{3+} was observed, was mainly associated with surface hydroxyl species, that is, silanols and aluminols. We revealed that the basal and edge surfaces of kaolin particles exhibit weakly mutual interacting hydroxyl groups. Some of those are similar to surface NFS groups, which lead to the molecular interaction of silica with biomembranes.[24] Besides surface chemistry effects, a variation of the fractality of the kaolin agglomerates may affect the surface available for the interaction and modulate membranolysis. For bentonite, a surface-driven membranolytic effect that involved weakly interacting surface OH could not be ruled out, but current data indicate a major effect due to CEC which generates local ionic imbalances that alter cellular homeostasis and induced membranolysis.

This new data provides a mechanistic basis for describing ion exchanger and non-exchanger LS interaction with living matter which is crucial for preventing possible adverse effects on human health and developing safe-by-design nanocomposite materials. Some of the mechanisms of interaction reported herein for RBC membrane lysis may be translated to other important interfacial phenomena of LS, including the antimicrobial activity of some aluminosilicate clays[11] and a variety of heterogeneous chemistry processes, such as grafting reactions[40] and atmospheric processes.[43]

4. Experimental Section

LS and Reference Particles: Kaolin (K1-4) and bentonite (B1-4) samples were kindly provided by the European Bentonite (EUBA) and European Kaolin and Plastic Clays (KPC) Associations. The selection criteria included: high external SSA (> 10 $m^2\ g^{-1}$), low QZ and cristobalite content (< 1%), similar size distribution (at least in the respirable range, < 5 µm), and industrial relevance. The commercial QZ Min-U-Sil 5 (QZ; US Silica Company, Berkeley Springs, WV), and the pyrogenic amorphous silica Aerosil OX50 (AS; Degussa) were also included in the study because of their well-known membranolytic activity.[24]

Chemical Reagents: When not otherwise specified, all reagents were purchased from Merck (Sigma-Aldrich). The water used was ultrapure Milli-Q water (Merck-Millipore).

SSA and Micropore Area: The SSA and micropore area of the particles were evaluated by the BET method based on N_2 adsorption-desorption at −196 °C, using an ASAP 2020 instrument (Micromeritics). Prior to measurements, samples were degassed at 80 °C for 12h in vacuum to remove adsorbed water and other gases. The total SSA was calculated according to the BET equation in the range P/P_0 = 0.05–0.30 (10 points). The external SSA (SSA_{ext}) was obtained by subtracting the micropore area, which was evaluated by the *t*-plot method, to the total SSA. For heated K3, only the adsorption isotherm was measured over the range P/P_0 = 0.05–0.25. Adsorption of Kr over the range P/P_0 = 0.05–0.20 (9 points) was applied for QZ as its expected SSA was low (≤ 5 $m^2\ g^{-1}$).

Particle Morphology and Minerochemical Composition: The morphology of dry particles was assessed by Field Emission Scanning Electron Microscopy (FE-SEM) with a TESCAN S9000G equipped with a Schottky FEG source. Images were taken at various magnifications and accelerating voltages, commonly between 5 and 15 kV, and 100 pA. Particles were deposited on conductive stubs covered with carbon tape and coated with chrome (5 nm) to prevent the electron beam from charging the sample. Elemental analysis was carried out by Energy Dispersive Spectroscopy (EDS) with an Oxford Aztec Ultim Max detector

(Oxford Instruments). Spectra were collected on at least twelve regions (ca. 650 μm^2) per sample, at 2–10k magnification, 10 kV accelerating voltage, and processed using Aztec suite (v. 4.2, Oxford Instruments). Crystallinity was assessed by XRD in Bragg–Brentano configuration with a Rigaku Miniflex 600 (Japan). Spectra were collected in the 2θ range (3 to 90°), with a step width of 0.02°, 3° min^{-1} of speed, and Cu Kα radiation at 40 kV and 15 mA. The diffractograms obtained were analyzed with the Rigaku PDXL 2 software. The chemical composition was obtained by atomic absorption spectrometry (AAS) or X-Ray Fluorescence analysis (XRF) with a Varian 250 Plus equipment or an Eagle IIIXPL spectrometer, respectively. Prior to the AAS determination, LS samples were melted in a muffle furnace at 1000 °C with lithium metaborate and solubilized in nitric acid.

Particle Size: Size analysis of particles dispersed in water and in milieu used for membranolysis (0.01 M PBS) was performed by Dynamic Light Scattering (DLS) and Flow Particle Image Analysis (FPIA). Kaolin and bentonite particles were preventively suspended in media (2 mg mL^{-1}) and sonicated for 1 min on ice with an ultrasonic probe (horn, 3 mm; frequency, 20 kHz; maximum power, 100 W; amplitude, 75 μm; Sonopuls HD 3100, Bandelin). The hydrodynamic diameter of diluted dispersions of particles (0.2 mg mL^{-1}in water or 0.01 M PBS) was measured by DLS with a Zetasizer Nano ZS (Malvern Instruments). To characterize the larger fraction, the size distribution was also assessed with a FPIA-3000S (Malvern Instruments; detection range: 0.8–160 μm). Diluted particle dispersions (1 mg mL^{-1}) were injected (ca. 5 mL) into the measurement cell, then stirred at 360 rpm. Particle images were captured using stroboscopic illumination and a charge-coupled device camera. Data were processed by the Sysmex FPIA software (version 00–13).

Surface Charge and pH: Particle surface charge (ζ potential) was measured by Electrophoretic Light Scattering (ELS; Zetasizer Nano ZS). Particles were suspended in 0.01 M PBS and sonicated for 1 min on ice with the ultrasonic probe then diluted to the concentration used for experiments (0.1 mg mL^{-1}). The pH of the particle dispersions or the leachates was checked with a digital in situ calibrated pH meter (827 pH Lab; Metrohm).

Membranolytic Activity: The membranolytic activity of kaolin and bentonite particles was assessed with the hemolysis test, using RBCs as a model of cell membranes. The RBCs were purified from sheep blood in Alsever's solution (Thermofisher) by centrifugation at 3000 × g for 2 min (Rotina 380R; Hettich) and washing three times with 0.9% NaCl (Eurospital). RBCs were suspended in 0.01 M PBS at the concentration of 5% by volume. Particles were dispersed at the initial concentration of 20 mg mL^{-1}in 0.01 M PBS and sonicated just before testing for 1 min on ice with the ultrasonic probe. Serial dilutions of the stock dispersion were then performed to the final concentrations used for experiments: 15, 10, 5, 2.5, 1.25, 0. 6, 0.3, and 0.1 mg mL^{-1} for kaolin; 15, 10, 5, 2.5, 1.25, 0. 6, 0.3, 0.1, 0.07, 0.05, 0.02, and 0.01 mg mL^{-1} for bentonite. Particle dispersions were distributed in quadruplicate in a 96-well plate (150 μL/well), and the RBC suspension was added (75 μL/well). Negative and positive controls consisted in PBS and 0.1% Triton-X 100 in PBS, respectively. The plate was incubated at 37 °C on an orbital plate shaker for 30 min and then centrifuged at 216 × g for 5 min. Supernatants were transferred to a new plate (75 μL/well), and the absorbance of the hemoglobin (Hb) released was determined at a wavelength of 540 nm on a UV/vis spectrophotometer (Ensight, Perkin Elemer) using the software Kaleido 2.0 (Perkin Elemer). Absorbance (Abs) values were converted to percentages of hemolysis according to Equation (1):

$$\%\ \text{hemolysis} = \frac{\text{Abs sample} - \text{Abs negative control}}{\text{Abs negative control} - \text{Abs positive control}} \times 100 \quad (1)$$

The LS samples did not adsorb the Hb released and measured in the test (data not shown). To determine the membranolytic activity of particle leachates, the kaolin and bentonite particles were suspended in PBS at a concentration that induced ca. 100% hemolysis (15 mg mL^{-1} for kaolin and 10 mg mL^{-1} for bentonite). Particle dispersions were sonicated on ice with the probe for 1 min, and incubated at 37 °C on an orbital plate shaker for 30 min. After incubation, particle dispersions were centrifuged at 12 000 × g for 10 min, the supernatant filtrated with InJ/Light syringes (Rays) and 0.2 μm PTFE membrane filters (Advantec), and hemolysis of the leachates was assessed as above described. The protocol to test the membranolytic activity of LS in presence of self-assembled PL, that is, 1,2-dioleyl-sn-glycero-3-phosphocholyne (DOPC) or 1,2-dioleoyl-sn-glycero-3-phospho-L-serine (DOPS) refers to ref. [31]. Briefly, PL stock dispersions were prepared by dispersing PL salt (Avanti Polar Lipids Inc.) in 0.01 M PBS at the initial concentration of 0.5 mg mL^{-1}. The PL dispersion was sonicated three times for 3 min using the ultrasound probe (horn, 3 mm; frequency, 20 kHz; power, 30W; Sonopuls HD 3100, Bandelin), stored for 10 min on ice, and centrifuged at 2500 x g for 10 min. The pellet was discarded, and the supernatant diluted to 0.3 mg mL^{-1} to verify the size of the supramolecular structures formed by DLS (Zetasizer Nano ZS). Serial dilutions of the PL stock dispersion were performed according to the final doses used for experiments and incubated for 30 min with particles. The particle dose causing 50% of hemolysis (EC50) was used after fitting the experimental points with a nonlinear regression curve based on the Hill equation (software GraphPad Prism 9.1.1). A group consisting just of particles (without PL) was added as reference group. PL at the highest concentration (0.1 mg mL^{-1}) was also incubated with RBCs (without LS particles) to demonstrate the absence of any hemolytic effect induced by PL. A suspension of 5% RBC was added to the mixture and the hemolytic activity was assessed after a further incubation of 30 min, as described above. The hemolytic activity of the LS particles in presence of DOPC was also assessed after washing particles incubated with DOPC. In detail, LS particles at their EC50 were incubated with DOPC (0.1 mg mL^{-1}) or just the vehicle (0.01 M PBS) for 30 min at 37 °C on a plate shaker. The mixture was centrifuged at 5000 x g for 10 min (Rotina 380), the supernatant removed, and the pellet used to test the hemolytic activity after washing three times with 1 mL of 0.01 M PBS and vortexing for 30 s. To check the effect of pH variation of the milieu on the membranolytic activity induced by bentonites, the pH of the leachates was adjusted to 7.4 (physiological pH) using 0.1 M HCl. Moreover, a negative control consisting of PBS at pH ca. 9 (basified with 0.1 M NaOH) was added. The hemolysis of the pH-adjusted leachates and PBS was assessed.

Determination of the Cation Exchange Capacity (CEC): The method for the direct CEC measurement by adsorption of Cu(II)-triethylenetetramine dye refers to ref. [44].

Determination of Cations Released by Particles: Dispersions of kaolin and bentonite particles were prepared in 0.01 M PBS (10 mg mL^{-1}, 10 mL) in triplicate, reproducing the same conditions and with the same separation techniques used to obtain the leachates for hemolysis test. PBS was filtered and used as reference. The concentration of ions in the leaching solution was assessed by ICP-OES with a Perkin–Elmer Optima 2000 DV ICP-OES spectrometer (Perkin Elmer) equipped with a cross-flow nebulizer placed inside a Scott spray chamber. One mL of each filtered solution was diluted (1:10) with a 1% nitric acid solution and the concentration of leached Si, Al, Mg, and Ca from the particles was assessed. Notably, it was not possible to measure the Na and K release due to their high content in the PBS used for the experiments. ICP Aristar (BDH) standard solutions in nitric acid for Si (10 000 mg L^{-1}), Mg, Ca, and Al (1000 mg L^{-1}) were used to prepare the calibrating solutions for ICP-OES analyses. The standard solutions used for the calibration curves were prepared in the same way as the samples, using PBS diluted 1:20 with a 1% nitric acid solution. Measurements of the standard solutions were regularly repeated after the measurements of every single experiment. Data reported were the average values of three independent measurements (corrected for the blank).

Heat Treatments of Kaolin: K3 (1g) was heated (rump up: 10 °C min^{-1}) in a muffle furnace for 2h at the reported *T* and allowed to cool at RT in the same furnace. Heated samples were stored in a glove box in Ar atmosphere (< 0.1 ppm water and O_2) prior to further measurements.

Thermogravimetric Analysis (TGA): The LS samples (ca. 15 mg) were heated from 30 to 1000 °C at 10 °C min^{-1} in a thermogravimetric balance (sensitivity 0.1 μg; Pyris 1 TGA, Perkin Elmer) under N_2 atmosphere. Results were analyzed with the Pyris Manager 11 software (Perkin Elmer) and reported as a weight percent loss and its derivative curve (dTG) as a function of the sample *T*. To simulate the isothermal treatments

designed to investigate kaolin surface hydroxyl distribution, isothermal TGA analysis at 300, 400, 450, 500, and 600 °C was also conducted.

Surface Hydroxyl Distribution: IR spectra were acquired at a resolution of 4 cm^{-1} with a Bruker Invenio R spectrometer equipped with a DTGS detector. The number of scans was adjusted to 64 to obtain a good signal-to-noise ratio. For collecting spectra in ATR mode, a Specac's Golden Gate single reflection diamond ATR accessory was employed. Conversely, to acquire IR spectra in transmission mode, the powders (ca. 50 mg) were pressed into self-supporting pellets and placed in special IR cells (QZ cell equipped with CaF_2 windows). The cell allows to perform in situ adsorption-desorption experiments by the connection to a conventional vacuum line (residual pressure < 1 x 10^{-3} mbar). The data were normalized by the optical density (mg cm^{-2} of pellet) in order to make differences in intensity independent of differences in the thickness of the pellets. To isolate the components due only to surface hydroxyl groups, pristine OH were converted into OD species by contact with D_2O molecules (99.90% D).[24] The resulting OD pattern was in the 2800–2200 cm^{-1} range. To ensure the completeness of the isotopic exchange of the surface OH groups, the following procedure was adopted: i) initial outgassing at beam temperature for 120 min and acquisition of the "OH outgassed spectrum"; ii) admission of D_2O vapor at 20 mbar followed by short outgassing; iii) repetition of point (ii) until spectral invariance (typically 5 cycles); iv) final outgassing for 120 min and acquisition of the "OD outgassed spectrum".

Statistical Analysis: Statistical parameters, including the number of independent experiments and statistical significance, are reported in the figures and figure legends. Unless otherwise stated, data were presented as mean ± SEM. Normally distributed data were analyzed by two-tailed unpaired Student's t-test, or one-way ANOVA followed by Dunnett's post hoc test, as appropriate. In all tests, a 95% confidence interval was used, for which differences with $p < 0.05$ were considered statistically significant. Statistical analysis was performed with the GraphPad Prism 9.3.1 software (GraphPad Software).

Supporting Information

Supporting Information is available from the Wiley Online Library or from the author.

Acknowledgements

This study was supported by the European Bentonite Association (EUBA) and the European Kaolin and Plastic Clays Association (KPC-Europe) (Brussels, Belgium) under the research contract "EUBeKa – Surface Hydroxyls and Membranolytic Screening of Bentonite and Kaolin Dusts". The authors are grateful to Prof. Alessandro Pacella (Dipartimento di Scienze della Terra, Laboratorio Rettorale Fibre e Particolato Inorganico, Sapienza Università di Roma, Italy) and Dr. Maria Rita Monterali (Agenzia Nazionale per le Nuove Tecnologie, l'Energia e lo Sviluppo Economico Sostenibile, Italy) for ICP-OES analysis and discussion, Prof. Giuliana Magnacca (Department of Chemistry, University of Turin) for assistance with BET analysis, and Dr. Maria Carmen Valsania and Dr. Erica Rebba for assistance with FE-SEM and EDX analyses.

Open access Funding provided by Universita degli Studi di Torino within the CRUI-CARE Agreement.

Conflict of Interest

The authors declare no conflict of interest.

Data Availability Statement

The data that support the findings of this study are available from the corresponding author upon reasonable request.

Keywords

bentonite, cation exchange, clay, hydroxyl groups, kaolin, membrane, silicate

Received: June 16, 2022
Revised: July 28, 2022
Published online:

[1] a) N. Z. Janković, D. L. Plata, *Environ. Sci.: Nano* **2019**, *6*, 2697; b) M. Connolly, Y. Zhang, S. Mahri, D. M. Brown, N. Ortuno, M. Jorda-Beneyto, K. Maciaszek, V. Stone, T. F. Fernandes, H. J. Johnston, *Food Chem. Toxicol.* **2019**, *126*, 178.
[2] A. Awasthi, P. Jadhao, K. Kumari, *SN Appl. Sci.* **2019**, *1*, 1076.
[3] Y. T. Zou, Y. Z. Hu, Z. W. Shen, L. Yao, D. Y. Tang, S. Zhang, S. Q. Wang, B. W. Hu, G. X. Zhao, X. K. Wang, *J. Environ. Sci.* **2022**, *115*, 190.
[4] L. Alves, E. Ferraz, J. A. F. Gamelas, *Adv. Colloid Interface Sci.* **2019**, *272*, 101994.
[5] H. H. Murray, *Appl. Clay Sci.* **1991**, *5*, 379.
[6] S. Maisanaba, S. Pichardo, M. Puerto, D. Gutierrez-Praena, A. M. Camean, A. Jos, *Environ. Res.* **2015**, *138*, 233.
[7] a) C. Viseras, R. Sánchez-Espejo, R. Palumbo, N. Liccardi, F. García-Villén, A. Borrego-Sánchez, M. Massaro, S. Riela, A. López-Galindo, *Clays Clay Miner.* **2021**, *69*, 561; b) M. I. Carretero, M. Pozo, *Appl. Clay Sci.* **2010**, *47*, 171.
[8] K. K. Chenab, B. Sohrabi, A. Jafari, S. Ramakrishna, *Mater. Today Chem.* **2020**, *16*, 100262.
[9] a) N. Khatoon, M. Q. Chu, C. H. Zhou, *J. Mater. Chem. B* **2020**, *8*, 7335; b) M. Massaro, C. G. Colletti, G. Lazzara, S. Riela, *J. Funct. Biomater.* **2018**, *9*, 58; c) D. Peixoto, I. Pereira, M. Pereira-Silva, F. Veiga, M. R. Hamblin, Y. Lvov, M. Liu, A. C. Paiva-Santos, *Coord. Chem. Rev.* **2021**, *440*, 213956; d) A. Murali, G. Lokhande, K. A. Deo, A. Brokesh, A. K. Gaharwar, *Mater. Today* **2021**, *50*, 276.
[10] a) J. I. Dawson, R. O. C. Oreffo, *Adv. Mater.* **2013**, *25*, 4069; b) J. K. Carrow, L. M. Cross, R. W. Reese, M. K. Jaiswal, C. A. Gregory, R. Kaunas, I. Singh, A. K. Gaharwar, *Proc. Natl. Acad. Sci. USA* **2018**, *115*, E3905; c) M. Mousa, N. D. Evans, R. O. C. Oreffo, J. I. Dawson, *Biomaterials* **2018**, *159*, 204.
[11] S. C. Londono, H. E. Hartnett, L. B. Williams, *Environ. Sci. Technol.* **2017**, *51*, 2401.
[12] a) Z. Adamis, R. Williams, International Programme on Chemical Safety. *Bentonite, kaolin and selected clay minerals*, World Health Organization, Geneva, Switzerland **2005**; b) K. Maciaszek, D. M. Brown, V. Stone, *Toxicol. In Vitro* **2022**, *78*, 105273; c) J. Nones, H. G. Riella, A. G. Trentin, J. Nones, *Appl. Clay Sci.* **2015**, *105–106*, 225.
[13] S. Scholz, J. W. Nichols, B. I. Escher, G. T. Ankley, R. Altenburger, B. Blackwell, W. Brack, L. Burkhard, T. W. Collette, J. A. Doering, D. Ekman, K. Fay, F. Fischer, J. Hackermüller, J. C. Hoffman, C. Lai, D. Leuthold, D. Martinovic-Weigelt, T. Reemtsma, N. Pollesch, A. Schroeder, G. Schüürmann, M. von Bergen, *Environ. Toxicol. Chem.* **2022**, *41*, 30.
[14] a) M. Wiemann, A. Vennemann, W. Wohlleben, *Nanomaterials* **2020**, *10*, 204; b) T. A. Stueckle, D. C. Davidson, R. Derk, T. G. Kornberg, L. Battelli, S. Friend, M. Orandle, A. Wagner, C. Z. Dinu, K. A. Sierros, S. Agarwal, R. K. Gupta, Y. Rojanasakul, D. W. Porter, L. Rojanasakul, *ACS Nano* **2018**, *12*, 2292.
[15] a) N. K. Verma, E. Moore, W. Blau, Y. Volkov, P. Ramesh Babu, *J. Nanopart. Res.* **2012**, *14*, 1137; b) A. Wagner, A. P. White, T. A. Stueckle, D. Banerjee, K. A. Sierros, Y. Rojanasakul, S. Agarwal, R. K. Gupta, C. Z. Dinu, *ACS Appl. Mater. Interfaces* **2017**, *9*, 32323.
[16] a) S. Manyai, J. Kabai, J. Kis, E. Suveges, M. Timar, *Med. Lav.* **1969**, *60*, 331; b) C. D. Woodworth, B. T. Mossman, J. E. Craighead, *Environ. Res.* **1982**, *27*, 190; c) W. E. Wallace, V. Vallyathan,

M. J. Keane, V. Robinson, *J. Toxicol. Environ. Health* **1985**, *16*, 415; d) V. Vallyathan, D. Schwegler, M. Reasor, L. Stettler, J. Clere, F. H. Y. Green, in *Inhaled Particles VI*, (Eds: J. Dodgson, R. I. McCallum, M. R. Bailey, D. R. Fisher), Pergamon Press **1988**; e) S. Geh, R. Yucel, R. Duffin, C. Albrecht, P. J. Borm, L. Armbruster, M. Raulf-Heimsoth, T. Bruning, E. Hoffmann, A. W. Rettenmeier, E. Dopp, *Arch. Toxicol.* **2006**, *80*, 98; f) E. J. Murphy, E. Roberts, L. A. Horrocks, *Neuroscience* **1993**, *55*, 597.

[17] a) T. P. Kennedy, R. Dodson, N. V. Rao, H. Ky, C. Hopkins, M. Baser, E. Tolley, J. R. Hoidal, *Arch. Biochem. Biophys.* **1989**, *269*, 359; b) S. Geh, T. Shi, B. Shokouhi, R. P. Schins, L. Armbruster, A. W. Rettenmeier, E. Dopp, *Inhalation Toxicol.* **2006**, *18*, 405.

[18] a) S. Maisanaba, D. Gutierrez-Praena, S. Pichardo, F. J. Moreno, M. Jorda, A. M. Camean, S. Aucejo, A. Jos, *J. Appl. Toxicol.* **2014**, *34*, 714; b) S. Lordan, J. E. Kennedy, C. L. Higginbotham, *J. Appl. Toxicol.* **2011**, *31*, 27; c) M. Baek, J.-A. Lee, S.-J. Choi, *Mol. Cell. Toxicol.* **2012**, *8*, 95.

[19] a) R. Davies, *Environ. Health Perspect.* **1983**, *51*, 249; b) W. E. Wallace, M. J. Keane, P. S. Mike, C. A. Hill, V. Vallyathan, E. D. Regad, *J. Toxicol. Environ. Health* **1992**, *37*, 391.

[20] a) M. Suwalsky, B. Norris, T. Kiss, P. Zatta, *Coord. Chem. Rev.* **2002**, *228*, 285; b) V. Hornung, F. Bauernfeind, A. Halle, E. O. Samstad, H. Kono, K. L. Rock, K. A. Fitzgerald, E. Latz, *Nat. Immunol.* **2008**, *9*, 847.

[21] a) A. Pacella, P. Ballirano, M. Fantauzzi, A. Rossi, C. Viti, L. Arrizza, E. Nardi, R. Caprioli, M. R. Montereali, *Minerals* **2021**, *11*, 914; b) P. Nunes, I. Roth, P. Meda, E. Féraille, D. Brown, U. Hasler, *Proc. Natl. Acad. Sci. USA* **2015**, *112*, E3104.

[22] a) H. H. Murray, in *Applied Clay Mineralogy. Occurrences, Processing and Application of Kaolins, Bentonites, Palygorskite-Sepiolite, and Common Clays*, Vol. *2*, Elsevier, Amsterdam **2007**; b) W. A. Deer FRS, R. A. Howie, J. Zussman, in *An Introduction to the Rock-Forming Minerals*, Mineralogical Society of Great Britain and Ireland, **2013**.

[23] P. F. Weck, E. Kim, C. F. Jové-Colón, *Dalton Trans.* **2015**, *44*, 12550.

[24] C. Pavan, R. Santalucia, R. Leinardi, M. Fabbiani, Y. Yakoub, F. Uwambayinema, P. Ugliengo, M. Tomatis, G. Martra, F. Turci, D. Lison, B. Fubini, *Proc. Natl. Acad. Sci. U. S. A.* **2020**, *117*, 27836.

[25] C. Pavan, M. Delle Piane, M. Gullo, F. Filippi, B. Fubini, P. Hoet, C. J. Horwell, F. Huaux, D. Lison, C. Lo Giudice, G. Martra, E. Montfort, R. Schins, M. Sulpizi, K. Wegner, M. Wyart-Remy, C. Ziemann, F. Turci, *Part. Fibre Toxicol.* **2019**, *16*, 32.

[26] D. L. Bish, R. B. Von Dreele, *Clays Clay Miner.* **1989**, *37*, 289.

[27] A. Viani, A. F. Gualtieri, G. Artioli, *Am. Mineral.* **2002**, *87*, 966.

[28] L. J. Michot, in *Developments in Clay Science*, Vol. *9* (Eds: R. Schoonheydt, C. T. Johnston, F. Bergaya), Elsevier, **2018**.

[29] F. Macht, K. Eusterhues, G. J. Pronk, K. U. Totsche, *Appl. Clay Sci.* **2011**, *53*, 20.

[30] E. Tombácz, M. Szekeres, *Appl. Clay Sci.* **2006**, *34*, 105.

[31] C. Pavan, M. J. Sydor, C. Bellomo, R. Leinardi, S. Cananà, R. L. Kendall, E. Rebba, M. Corno, P. Ugliengo, L. Mino, A. Holian, F. Turci, *Colloids Surf., B.* **2022**, *217*, 112625.

[32] D. Di Giuseppe, S. Scarfì, A. Alessandrini, A. M. Bassi, S. Mirata, V. Almonti, G. Ragazzini, A. Mescola, M. Filaferro, R. Avallone, G. Vitale, V. Scognamiglio, A. F. Gualtieri, *Toxicology* **2022**, *466*, 153081.

[33] F. M. Kregenow, *Annu. Rev. Physiol.* **1981**, *43*, 493.

[34] a) D. W. Oscarson, G. E. Van Scoyoc, J. L. Ahlrichs, *Clays Clay Miner.* **1986**, *34*, 74; b) D. W. Oscarson, G. E. van Scoyoc, J. L. Ahlrichs, *J. Pharm. Sci.* **1981**, *70*, 657.

[35] E. Di Ianni, P. Møller, A. Mortensen, J. Szarek, P. A. Clausen, A. T. Saber, U. Vogel, N. R. Jacobsen, *Nanotoxicology* **2020**, *14*, 869.

[36] O. V. Bondar, D. V. Saifullina, I. I. Shakhmaeva, I. I. Mavlyutova, T. I. Abdullin, *Acta Nat.* **2012**, *4*, 78.

[37] J. A. Snyder, J. D. Madura, *J. Phys. Chem. B* **2008**, *112*, 7095.

[38] H. Wang, C. Li, Z. Peng, S. Zhang, *J. Therm. Anal. Calorim.* **2011**, *105*, 157.

[39] a) C. E. White, J. L. Provis, T. Proffen, D. P. Riley, J. S. J. van Deventer, *Phys. Chem. Chem. Phys.* **2010**, *12*, 3239; b) Q. Wan, F. Rao, S. Song, *J. Non-Cryst. Solids* **2017**, *460*, 74.

[40] J. T. Kloprogge, *Spectroscopic Methods in the Study of Kaolin Minerals and Their Modifications*, Springer Nature, Cham, Switzerland **2019**.

[41] S. Mányai, J. Kabai, J. Kis, É. Süveges, M. Timár, *Environ. Res.* **1970**, *3*, 187.

[42] J. Davidovits, *J. Ceram. Sci. Technol.* **2017**, *08*, 335.

[43] S. K. Sihvonen, K. A. Murphy, N. M. Washton, M. B. Altaf, K. T. Mueller, M. A. Freedman, *Z. Phys. Chem.* **2018**, *232*, 409.

[44] A. Decher, S. Ramrattan, *Int. J. Metalcast.* **2021**, *15*, 373.